# Polymer Chemistry

Accepted Manuscript

This article can be cited before page numbers have been issued, to do this please use: C. Cuscó Marigó, J. Garcia, E. Nicolas, P. Rocas and J. Rocas, *Polym. Chem.*, 2016, DOI: 10.1039/C6PY01275B.




ROYAL SOCIETY OF CHEMISTRY

www.rsc.org/polymers

View Article Online
DOI: 10.1039/C6PY01275B

# Multisensitive drug-loaded polyurethane/polyurea nanocapsules with pH-synchronized shell cationization and redox-triggered release

Cristina Cuscó,*[1,2] Jordi Garcia,[2] Ernesto Nicolás,[2] Pau Rocas[1] and Josep Rocas*[1]

[1] Nanobiotechnological Polymers Division, Ecopol Tech, S.L., El Foix Business Park, Indústria 7, 43720 L'Arboç del Penedès, Tarragona, Spain

[2] Organic Chemistry Section, Inorganic and Organic Chemistry Department, Faculty of Chemistry, CIBERobn and IBUB, University of Barcelona, Martí i Franquès 1-11, 08028 Barcelona, Spain





## 1. Abstract

An industrially scalable and versatile method to prepare amphiphilic and amphoteric multifunctionalized polyurethane/polyurea nanocapsules (NCs) is presented. Firstly, a prepolymer is prepared from a diisocyanate, which reacts with different functional diols and diamines, leading to a self-emulsifiable reactive product. Secondly, this prepolymer is used to nanoemulsify the desired hydrophobic drug in aqueous conditions. In this step, the prepolymer generates a self-organized drug/water interface driven by its hydrophobic/hydrophilic balance (HLB) and allows a stable and size-controlled nanoemulsion without external surfactants. Finally, the process is completed with the addition of a crosslinker, which converts the nanodroplets into robust nanocapsules. The process allows chemical versatility, high encapsulation yields and remarkable drug loading content. The nanocapsules have a monomodal particle size distribution, a roughly round shape and amphoteric properties, which make the nanocapsules very sensitive to small pH changes occurring between blood or extracellular fluids of normal cells and the extracellular tumor microenvironment. Such effect is intended to increase the stealthiness of the nanocapsule through a neutral hydrophilic corona in physiological conditions and also to enhance cell internalization in tumor cells via surface self-cationization. Fluorescence studies show prolonged stability under physiological conditions and specific degradability through a redox-triggered process involving reduced L-glutathione (L-GSH).

View Article Online
DOI: 10.1039/C6PY01275B



## 2. Introduction

Nowadays, cancer is the second major cause of death in developed countries, following coronary diseases and stroke. Indeed, cancer is responsible for one in three premature deaths from chronic illnesses and the prognostics suggest an ever-increasing cancer burden in low and middle-income countries, reaching 20 million of new diagnosed cases by 2030.[1-5] Therefore, it is evident that urgent new resource-contingent strategies are needed to reduce cancer incidence worldwide.[6]

Continued progress has been made in revealing cellular, genetic and molecular fundamentals of cancer. In fact, different disciplines have been combining forces for a long time to design new drugs and alternative therapies against this complex disease.[7] Unfortunately, these efforts are most of the times not effectively translated into clinical applications because even the more active new drugs still lack aqueous solubility, selectivity towards tumor cells and, as a consequence, insufficient drug concentration is provided at the targeting site. This leads to a low therapeutic index, undesirable side effects and, in some cases, multidrug resistance, which worsen the patients' quality of life.[8-10]

In order to overcome these limitations, a wide range of novel drug delivery systems (DDS) with improved efficacy and negligible toxicity are being developed, especially in the field of nanotechnology.[11-15] Nanoparticle-based drugs have unique properties due to their small size, large surface-to-volume ratios and the possibility to functionalize their surface, resulting into improved pharmacokinetic and pharmacodynamic profiles compared to free drugs.[8, 16-18] Despite this encouraging scenario, most of the advances in this field do not materialize into commercial products. On one hand, this is due to the lack of robustness of the nanosystems (low structural consistency), which leads to unspecific drug leakage; low selectivity owing to invariable surface characteristics and limited encapsulation efficiency and drug loading, among others. On the other hand, difficulties in the scale-up of multistep processes requiring several purification steps also hamper the industrial development of multifunctional systems.

With these problems in mind, we have developed an easily scalable process to prepare multifunctional polyurethane/polyurea prepolymers, which can be subsequently used to nanoencapsulate hydrophobic drugs in aqueous conditions. In this regard, the chemical versatility behind this method has allowed the incorporation of a broad range of potential functionalities, such as biodegradable bonds, targeting ligands, charged moieties and dangling chains of different polarity.[19] The prepolymers containing such functionalities create ordered

View Article Online
DOI: 10.1039/C6PY01275B



shells due to their HLB and self-stratified at the oil-water interface leading to multiwalled structures.[20-22]

In the present paper we present a further step in this direction by developing smarter nanocapsules having a broader applicability to other drugs, more controlled particle size, higher robustness, very specific degradability and, more importantly, tunable surface properties. In this regard, we have generated amphiphilic and amphoteric nanocapsules sensitive to narrow pH changes as a tool to specifically target and permeate tumor cells. This special feature is achieved via functionalization with two specific monomers, a multicationic and an anionic ionomer. Their intrinsic acid-base properties lead to a synchronized effect at the target pH range between physiological conditions and tumor microenvironment. Moreover, these nanostructures have been finely designed to improve other properties, such as encapsulation yield, drug loading, structural stability and specific biodegradability by reductive biomolecules, such as cytosolic enzymes, coenzymes and peptides found intratumorally .[23, 24]

# 3. Materials and methods

## 3.1. Chemicals

Isophorone diisocyanate (IPDI) was purchased from Quimidroga (Barcelona, Spain), YMER N-120 was kindly supplied by Perstorp (Perstorp, Sweden) and *N*-tallow-1,3-propylenediamine (Genamin TAP 100D) was kindly provided by Clariant (Barcelona, Spain). *N*-(3-dimethylaminopropyl)-*N,N*-diisopropanolamine (Jeffcat DPA) was purchased from Huntsman Corporation (Barcelona, Spain), L-lysine hydrochloride, tetrahydrofuran and 2-hydroxyethyl disulfide (DEDS) were provided from Panreac (Barcelona, Spain) and diethylenetriamine (DETA) was obtained from BASF (Barcelona, Spain). HL3 and HL4 were kindly provided by Prof. Gamez's group. Unless stated otherwise, all other reagents, including HSA and BSA, were purchased from Sigma-Aldrich (St Louis, MO, USA).

## 3.2. Experimental methods

### *3.2.1. Synthesis of the amphiphilic cationic prepolymer (P1)*

DEDS (0.381 g, 4.9 meq), YMER N-120 (4.413 g, 8.5 meq) and Jeffcat DPA (0.371 g, 3.4 meq) were added into a previously purged three-necked round bottom flask at room temperature. When the mixture was homogeneous, IPDI (3.170 g, 28.5 meq) was added into the reaction vessel under gentle mechanical stirring. The polyaddition reaction was kept under these

View Article Online
DOI: 10.1039/C6PY01275B



conditions until the –N=C=O stretching band was stabilized, checked by FT-IR (ATR). At this point, dry THF (10 mL) was added into the reaction mixture in order to fluidify the polymer. On the other hand, Genamin TAP 100D (2.476 g, 14.7 meq) was dissolved with dry THF (10 mL) into another three-necked round bottom flask, which had previously been purged and pre-cooled to 4 °C. The first reaction mixture (-N=C=O reactive) was added onto the aminic solution under smooth mechanical stirring. The reaction was monitored by FT-IR (ATR) until –N=C=O stretching band had completely disappeared. The composition of this polymer in % by weight is shown in Figure S1.

### *3.2.2. Synthesis of drug-loaded amphiphilic and amphoteric polyurethane/polyurea nanocapsules (P1-drug-loaded amphoteric NCs)*

IPDI (30.2 mg, 0.27 meq) was added into a three-necked round bottom flask equipped with a mechanical stirrer, precooled at 4 °C and purged with $N_2$. Next, a mixture of the drug, the amphiphilic polymer P1 (0.659 g) and dry THF (1 mL) were added into the vessel and left for homogenization for 30 min. At this point, L-lysine (7.6 mg, 0.09 meq) was added and the polyaddition reaction was controlled after 45 min by FT-IR (ATR). Then, the organic mixture was emulsified with of pure cold water (15 mL) and finally DETA (4.2 mg, 0.12 meq) was added in order to generate crosslinked nanocapsules from the nanodroplets present in the emulsion. This polyaddition reaction was monitored by FT-IR and pH measurements. When the nanocapsules were formed, the THF was removed from the reactor, the pH was adjusted using diluted aqueous HCl and the nanocapsules were dialyzed against pure water during 72 h for further characterization (12000-14000 MWCO).

### *3.2.3. Synthesis of amphiphilic and amphoteric blank polyurethane/polyurea nanocapsules (P1-unloaded amphoteric NCs)*

Blank polyurethane/polyurea nanocapsules were prepared as previously described in section 3.2.2 with the only difference that no drug was added along with P1. The rest of the procedure was followed without any other modification.

### *3.2.4. Synthesis of DiO-loaded amphiphilic amphoteric polyurethane/polyurea nanocapsules (P1-DiO-loaded amphoteric NCs)*

DiO-loaded polyurethane/polyurea nanocapsules were prepared as previously described in section 3.2.2, using in this case DiO (4 mg, 4.54 meq) as a lipophilic tracer added along with P1. The rest of the procedure was followed without any other modification.

View Article Online
DOI: 10.1039/C6PY01275B



### *3.2.5. Synthesis of DiI-loaded amphiphilic amphoteric polyurethane/polyurea nanocapsules (P1-DiI-loaded amphoteric NCs)*

DiI-loaded polyurethane/polyurea nanocapsules were prepared as previously described in section 3.2.2, using in this case DiI (4 mg, 4.02 meq) as a lipophilic tracer added along with P1. The rest of the procedure was followed without any other modification.

### *3.2.6. Synthesis of drug-loaded amphiphilic and cationic polyurethane/polyurea nanocapsules (P1-drug-loaded cationic NCs)*

IPDI (30.2 mg, 0.27 meq) was added into a pre-cooled (4 °C) and purged with $N_2$ three-necked round bottom flask equipped with a mechanical stirrer. Then, a mixture of the drug and the amphiphilic polymer P1 (0.659 g) in dry THF (1 mL) was added into the vessel and left for homogenization for 30 min. The resulting organic mixture was emulsified with pure cold water (15 mL) and DETA (4.2 mg, 0.12 meq) was added in order to generate crosslinked nanocapsules from the nanodroplets present in the emulsion. The polyaddition reaction was monitored by FT-IR and pH measurements. When the nanocapsules were formed, THF was removed under vacuum, the pH was adjusted using diluted aqueous HCl solution and the nanocapsules were dialyzed against pure water during 72 h for further characterization (12000-14000 MWCO).

### *3.2.7. Synthesis of the amphiphilic prepolymer (P2)*

DEDS (0.381 g, 4.9 meq) and YMER N-120 (4.413 g, 8.5 meq) were added into a previously purged three-necked round bottom flask at room temperature. When the mixture was homogeneous, IPDI (2.524 g, 22.7 meq) was added under gentle mechanical stirring and the polyaddition reaction was kept under these conditions until -N=C=O stretching band was stabilized, checked by FT-IR (ATR). Then, dry THF (10 mL) was added into the reaction mixture in order to fluidify the polymer. On the other hand, Genamin TAP 100D (1.979 g, 11.7 meq) was dissolved with dry THF (10 mL) into another three-necked round bottom flask that had previously been purged and pre-cooled at 4 °C. The first reaction mixture was added dropwise into the aminic solution under smooth mechanical stirring and the reaction was monitored by FT-IR (ATR) until no detection of the -N=C=O stretching band. The composition of this polymer in % by weight is shown in Figure S1.

View Article Online
DOI: 10.1039/C6PY01275B



### *3.2.8. Synthesis of drug-loaded amphiphilic and anionic polyurethane/polyurea nanocapsules (P2-drug-loaded anionic NCs)*

IPDI (30.2 mg, 0.27 meq) was added into a pre-cooled (4 °C) and purged with $N_2$ three-necked round bottom flask equipped with a mechanical stirrer. Next, a mixture of the drug and the amphiphilic polymer P2 (0.659 g) in dry THF (1 mL) was added and the resulting suspension was left for homogenization for 30 min. Then, L-lysine (7.6 mg, 0.09 meq) was added and the polyaddition reaction was controlled after 45 minutes by FT-IR (ATR). The resulting organic mixture was emulsified with pure cold water (15 mL) and DETA (4.2 mg, 0.12 meq) was added in order to generate crosslinked nanocapsules from the nanodroplets present in the emulsion. The polyaddition reaction was monitored by FT-IR and pH measurements. When the nanocapsules were formed, THF was removed under vacuum, the pH was adjusted using diluted aqueous HCl solution and the nanocapsules were dialyzed against pure water during 72 h for further characterization (12000-14000 MWCO).

### *3.2.9. Synthesis of non-labile amphiphilic and amphoteric prepolymer (P3)*

1,6-hexanediol (0.29 g, 4.9 meq), YMER N-120 (4.413 g, 8.5 meq) and Jeffcap DPA (0.371 g, 3.4 meq) were added into a previously purged three-necked round bottom flask at room temperature. When the mixture was homogeneous, IPDI (3.170 g, 28.5 meq) was added under gentle mechanical stirring and the polyaddition reaction was kept under these conditions until –N=C=O stretching band was stabilized, checked by FT-IR (ATR). Then, dry THF (10 mL) was added into the reaction mixture in order to fluidify the polymer. On the other hand, Genamin TAP 100D (2.476 g, 14.7 meq) was dissolved with dry THF (10 mL) into another three-necked round bottom flask that had previously been purged and pre-cooled at 4 °C. The first reaction mixture was added dropwise to the aminic solution under smooth mechanical stirring and the reaction was monitored by FT-IR (ATR) until no detection of the -N=C=O stretching band. The composition of this polymer in % by weight is shown in Figure S1.

### *3.2.10. Synthesis of non-labile drug-loaded amphiphilic and amphoteric polyurethane/polyurea nanocapsules (P3-non-labile drug-loaded NCs)*

IPDI (30.2 mg, 0.27 meq) was added into a three-necked round bottom flask equipped with a mechanical stirrer, pre-cooled at 4 °C and purged with $N_2$. Next, a mixture of the drug, the amphiphilic polymer P3 (0.659 g) and dry THF (1 mL) were added into the vessel and left for homogenization for 30 min. At this point, L-lysine (7.6 mg, 0.09 meq) was added and the polyaddition reaction was controlled after 45 min by FT-IR (ATR). Then, the organic mixture was emulsified with of pure cold water (15 mL) and finally DETA (4.2 mg, 0.12 meq) was added

View Article Online
DOI: 10.1039/C6PY01275B



in order to generate crosslinked nanocapsules from the nanodroplets present in the emulsion. This polyaddition reaction was monitored by FT-IR and pH measurements. When the nanocapsules were formed, the THF was removed from the reactor, the pH was adjusted using diluted aqueous HCl and the nanocapsules were dialyzed against pure water during 72 h for further characterization (12000-14000 MWCO).

#### *3.2.11. Synthesis of non-labile DiO-loaded amphiphilic and amphoteric polyurethane/polyurea nanocapsules (P3-non-labile DiO-loaded NCs)*

DiO-loaded non-labile polyurethane/polyurea nanocapsules were prepared as previously described in section 3.2.10, using in this case DiO (4 mg, 4.54 meq) as a lipophilic tracer added along with P3. The rest of the procedure was followed without any other modification.

#### *3.2.12. Synthesis of non-labile DiI-loaded amphiphilic and amphoteric polyurethane/polyurea nanocapsules (non-labile DiI-loaded NCs)*

DiI-loaded non-labile polyurethane/polyurea nanocapsules were prepared as previously described in section 3.2.10, using in this case DiI (4 mg, 4.02 meq) as a lipophilic tarcer added along with P3. The rest of the procedure was followed without any other modification.

### 3.3. Analytical techniques

#### *3.3.1. Infrared spectra*

IR spectra were performed in a Smart iTR (Nicolet iS10, Thermo Scientific). For the monitoring of solvent-based samples, one drop was deposited onto the diamond crystal and the solvent was left to dry by evaporation. For the reaction control after emulsification, IR spectra were recorded from a dry film of the sample.

#### *3.3.2. pH measurements*

The pH of the emulsion was determined right after the crosslinker was added and at different time intervals until the last polyaddition reaction was complete. All the determinations were carried out in a pH-meter HI 2211 pH/ORP-Meter (HANNA Instruments) equipped with a pH electrode Crison 5029 and a temperature probe.

#### *3.3.3. Lyophilization and redispersion procedures*

Previously dialyzed samples were lyophilized and redispersed in the desired solvent depending on the characterization method. For organic solvents, the dry samples were immediately dissolved with no need of stirring; in the case of aqueous buffers or ultrapure water, the dry samples were redispersed by vigorous magnetic stirring overnight.

View Article Online
DOI: 10.1039/C6PY01275B



#### *3.3.4. Dynamic Light Scattering (DLS)*

The size distribution of the nanocapsules was analyzed on a Zetasizer Nano-ZS90 (Malvern) in pure water at 25 °C (1 mg/mL).

#### *3.3.5. Zeta potential measurements (Z-potential)*

The Z-potential of the nanocapsules was analyzed on a Zetasizer Nano-ZS90 (Malvern) in pure water at 25 °C (5 mg/mL) at different pH values.

#### *3.3.6. Transmission Electron Microscopy (TEM)*

The morphology of nanocapsules and the *in-vitro* degradation in presence of reduced L-glutathione (L-GSH) were studied in a Jeol JEM 1010 (Peabody, MA, USA). A 200 mesh copper grid coated with 0.75% FORMVAR was deposited on 6 µL of a suspension of nanocapsules in water (10 mg/mL) for 1 min. Excess of sample was removed by contact with ultra pure water for 1 min and the grid was deposited on a drop of uranyl acetate 2 % w/w in water for 1 min. The excess of uranyl acetate was removed and the grid was air-dried for at least 3 h prior to measurement.

For *in-vitro* degradation experiments, 150 µL of a suspension of nanocapsules in water (20 mg/mL) were added into a freshly prepared solution of reduced L-GSH in PBS (final glutathione concentration of 10 mM). The mixture was incubated at 37 °C for 24, 48, 72 and 96 h.

#### *3.3.7. Atomic Force microscopy (AFM)*

AFM analyses were performed using a atomic force microscope (AFM Multimode 8 with electronics Nanoscope V, Bruker) in Quantitative nanoMechanical (QNM) mode using a rectangular-shaped silicon cantilever with a pyramidal tip curvature of 8 nm and a nominal spring constant of 200 N/m (TAP525, Bruker). Mica discs were of muskovita from Ted Pella, EEUU.

#### *3.3.8. UV-Vis measurements*

To measure the entrapment efficiency (EE) and drug loading (DL) of nanocapsules, UV-Vis measurements were performed in a Cary 500 Scan (Varian) after dissolving a desired amount of dried nanocapsules in an exact volume of solvent. The measurements were done in triplicate, and the DL (%) and EE (%) were calculated from a calibration curve. DL (%) and EE (%) formulae are shown in the Supplementary Information section.

View Article Online
DOI: 10.1039/C6PY01275B



#### *3.3.9. Förster Resonance Energy Transfer (FRET) with labile nanocapsules. In vitro degradation experiments.*

Experiments were carried out using a stock solution of DiO and DiI at 7.5 μg/mL in PBS (pH 7.4) in order to study the release kinetics of hydrophobic molecules in different media. All measurements were performed in a Photon Technology International fluorometer (Birminghan, NJ, USA) by exciting the donor (DiO) at 484 nm and recording the emission spectrum from 495 to 650 nm. The experiments were carried out at a fixed temperature of 37 °C and constant magnetic stirring for 96 h.

##### *3.3.9.1. Control assay with Phosphate Buffer Saline (PBS)*

To study the release kinetics of hydrophobic molecules in an aqueous buffer, 16 μL of each stock solution were diluted to 3 mL with fresh PBS. In order to have a complete profile of the kinetics release of the system in this medium, the first measurements were performed every 30 min until 2 h of experiment. Afterwards, the delay between measurements was extended.

##### *3.3.9.2. Assay with an aqueous solution of Human Serum Albumin (HSA)*

The control experiment was repeated using a 40 mg/mL solution of HSA in PBS. The rest of the assay was followed with no other modification.

##### *3.3.9.3. Assay with an aqueous solution of Bovine Serum Albumin (BSA)*

The control experiment was repeated using a 40 mg/mL solution of BSA in PBS. The rest of the assay was followed with no other modification.

##### *3.3.9.4. Assay with reduced L-glutathione (L-GSH)*

The experiment was carried out under the same conditions that in the control experiment for the first 2 h. Then, the required amount of L-GSH was added into the cell to reach a concentration of 10 mM. In order to have a complete profile of the kinetics release of the system in this reductive medium, the first measurements were taken every 30 min for 2 h. Afterwards, the delay between measurements was extended.

#### *3.3.10. Förster Ressonance Energy Transfer (FRET) with non-labile nanocapsules. Assay with reduced L-glutathione (L-GSH). In vitro degradation experiments.*

The experiment was carried out using non-labile DiO- and DiI-loaded nanocapsules following the procedure described in 3.3.9.4.

View Article Online
DOI: 10.1039/C6PY01275B



## 4. Results and discussion

Our synthetic process started with the preparation of the amphiphilic prepolymer and finished with the nanoencapsulation of the hydrophobic drug. In order to clarify the whole method, a scheme with all the steps involved is presented (Scheme 1).

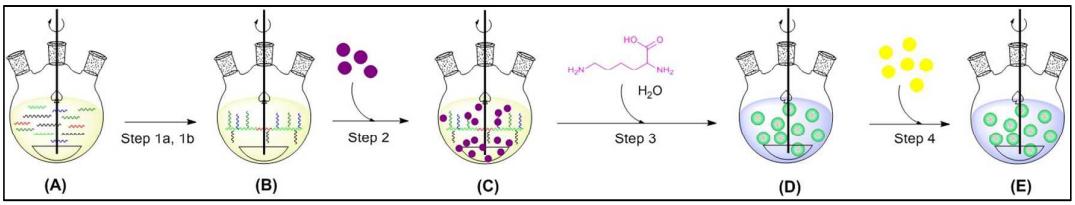


**Sch. 1**. Preparation of the amphiphilic polymer and subsequent nanoencapsulation of hydrophobic drugs.

First of all, the monomers were loaded into a three-necked flask and the polyaddition reactions started (A); once the amphiphilic prepolymer was formed (B), the desired hydrophobic drug represented in purple dots (paclitaxel, curcumin, HL3 and HL4 [25]) was added and the reaction mixture was left for homogenization (C); next, an aminic ionomer was introduced and cold water was added dropwise to turn the organic phase into an oil in water (o/w) nanoemulsion (D); finally, a polyamine (yellow dots) was added and the nanodroplets were converted into robustly crosslinked nanocapsules (E). During this process, and before the final crosslinking, the components forming the nanocapsule self-assemble and self-stratify according to the hydrophobic gradient created from the inner core containing the lipophilic drug to the hydrophilic surface of the nanocapsule, which is in direct contact with the aqueous phase. Therefore, the hydrophobic groups will be oriented to the inside whereas the hydrophilic or charged groups will point to the exterior. Each step of the process is shown in more detail in the Supplementary Information (Figure S2).

The amphiphilic prepolymer contains aliphatic side chains (from Genamin TAP 100D), which contribute to the drug solubilization and stabilization through hydrophobic interactions; poly(ethylene oxide) repeating units (from YMER N-120) provide the necessary hydrophilicity to allow a correct emulsification of the organic matrix (drug and polymer) in water. An appropriate prepolymer composition with an adjusted HLB is of crucial important to achieve self-emulsification and to avoid high speed stirring. As a consequence, the presence of external emulsifiers is avoided during the nanoencapsules formation. Additionally, it is also essential to guarantee a defined and stable o/w interface because otherwise a transfer of matter from small to large particles would take place to reduce the overall free energy associated with the particle-matrix interfacial area (Ostwald ripening effect).[26] This means that a correct

View Article Online
DOI: 10.1039/C6PY01275B



prepolymer composition also ensures that the nanodroplets remain stable during emulsification and do not grow to a larger size.

Besides lipophilic and hydrophilic side chains, the amphiphilic prepolymer also contains disulphide bonds that make the system biodegradable in reductive conditions. Finally, the presence of two specific ionomers, which are dicationic and anionic, on the polymeric shell modulates the surface charge of the nanocapsule depending on external pH. Figure 1 shows an illustrative example of the structural organization of the nanocapsule: the core is composed of the hydrophobic moieties of the prepolymer (fatty side chains and the lipophilic drug), the shell contains the crosslinked prepolymer, including disulfide bonds, and the hydrophilic fractions of the prepolymer (polyethyleneglycol repeating units, carboxylic acids and cationizable amines) are placed in the exterior aqueous phase.

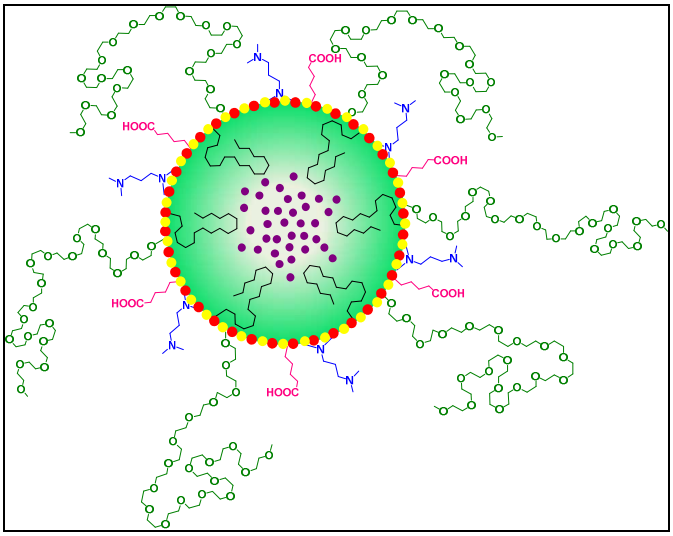


**Fig. 1.** The structure of a nanocapsule, including the orientation of the hydrophobic and hydrophilic fractions of the prepolymer.

The monitoring of polyaddition reactions was performed by FT-IR in all syntheses. Two illustrative examples are shown in Figure S3 and Figure S4, which correspond, respectively, to the synthesis of the amphiphilic prepolymer (P1) and the synthesis of drug-loaded amphiphilic and amphoteric polyurethane/polyurea nanocapsules (P1-drug-loaded amphoteric NCs).

In the case of the amphiphilic polymer, FT-IR spectra of step 1a, 1b and 2 of the synthetic process indicated a successful polyaddition reaction between DEDS, YMER N-120, Jeffcat DPA and IPDI, showing a significant decrease of the isocyanate asymmetric stretching band at 2253 $cm^{-1}$. Simultaneously, an increase of the carbonyl stretching band (1713 $cm^{-1}$), the CN/NH stretching band (1536 $cm^{-1}$) and the NCOO/COC asymmetric stretching band (1242 $cm^{-1}$) prove the polyurethane formation. In the second polyaddition reaction, which occurred between

View Article Online
DOI: 10.1039/C6PY01275B



remaining IPDI and Genamin TAP 100D, the isocyanate asymmetric stretching band completely disappeared, a new carbonyl stretching band at 1627 $cm^{-1}$ appeared and an increase of the C-N stretching band (Amide II) at 1536 $cm^{-1}$ could be detected due to polyurea formation.

In the case of steps 3 and 4 (synthesis of drug-loaded amphiphilic and amphoteric polyurethane/polyurea nanocapsules, P1-drug-loaded amphoteric NCs), FT-IR spectra confirmed the polyaddition reaction between IPDI and L-lysine, since the isocyanate asymmetric stretching band at 2253$cm^{-1}$ decreased while the carbonyl stretching band at 1627 $cm^{-1}$ and C-N stretching band (Amide II) at 1536 $cm^{-1}$ increased. Then, after the emulsification step, the monitoring of the polyaddition between remaining IPDI and the polyamine (DETA) indicated completion of the reaction, since the isocyanate asymmetric stretching band disappeared, together with another increase of the carbonyl stretching band at 1627 $cm^{-1}$ and C-N stretching band (Amide II) at 1536 $cm^{-1}$.

The crosslinking step (addition of DETA) is also controlled by pH changes in the reaction medium, indicating amine consumption (Figure S5).

The morphology of the nanocapsules was analyzed by Transmission Electron Microscopy (TEM) and Atomic Force Microscopy (AFM) and size distribution was evaluated by Dynamic Light Scattering (DLS). TEM micrographs of HL4-loaded NCs showed a roughly round shape and homogeneous particle size while DLS measurements demonstrated a narrow monomodal particle size distribution centered approximately at 20 nm. Standard deviation (SD) and polydispersity index (PDI) were low in all cases. Other TEM and AFM micrographs are shown in Figure S6 and Figure S7.

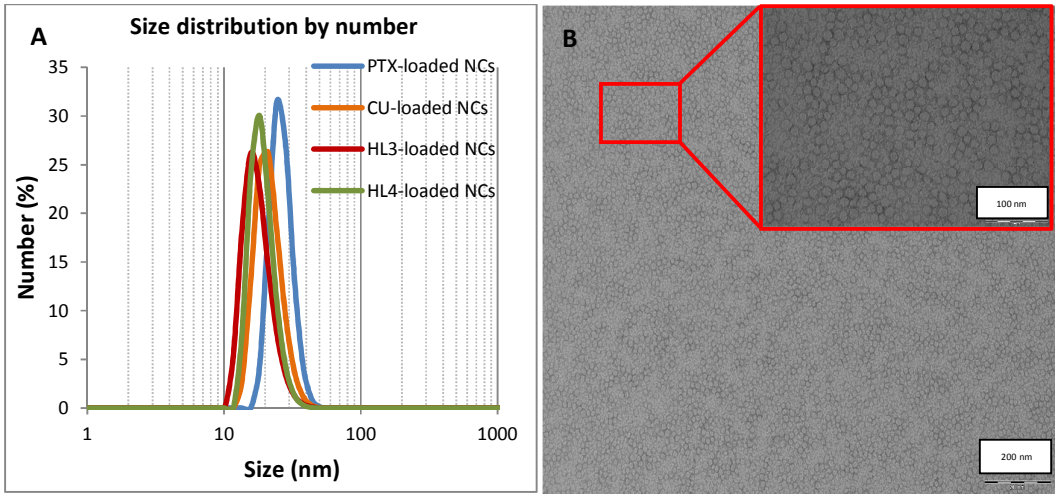

View Article Online
DOI: 10.1039/C6PY01275B



| C Sample name | Diameter (nm) | SD (nm) | PDI |
|---|---|---|---|
| PTX-loaded NCs | 23.254 | 5.039 | 0.263 |
| CU-loaded NCs | 20.080 | 5.030 | 0.155 |
| HL3-loaded NCs | 16.513 | 4.153 | 0.274 |
| HL4-loaded NCs | 17.340 | 4.093 | 0.101 |

**Fig. 2**. A) Particle size distribution of paclitaxel-, curcumin-, HL3- and HL4-loaded nanocapsules measured by DLS. B) TEM micrograph of HL4-loaded NCs (scale bar: 200 nm) including a zoom of a specific zone (scale bar: 100 nm). C) Statistical analysis of each kind of NCs including SD and PDI.

Besides morphological studies and size measurements, we also evaluated the modulation of the surface properties as a tool to specifically target cancer cells.

According to previous reports, neutral or slightly anionic nanocapsules have longer blood life-times and lower mononuclear phagocyte system uptake than their positively charged analogues. Additionally, hydrophilicity plays also an important role, since it provides an aqueous corona around the nanocarriers that shields them from to the complement system, making them more sterically stabilized and stealth.[27-30]

While hydrophilic nanocarriers are in the blood stream (pH around 7.4), they can eventually extravesate and slowly accumulate into abnormally vascularized tumor tissues due to their nanometric size.[31-35] In this environment, the pH becomes more acidic (pH= 5.8-6.9) due to high rate of glycolysis under aerobic or anaerobic conditions, poor lymphatic drainage, high interstitial pressure and inadequate blood supply near the tumor tissues.[36, 37] This pH change triggers a modification of the surface charge of the nanocapsules, becoming cationic entities. This change stimulates local accumulation and cell internalization, since they can bind to negatively charged groups on the cell surface (e.g. sialic acid) and translocate across the plasma membrane leading to high levels of cell penetration.[38, 39] Nevertheless, ligand-bearing nanoparticles exhibiting highly positive Z-potentials are disadvantaged by their non-specific binding to cell membranes driven by electrostatic interactions.[38]

To achieve this dual performance, we have decorated the nanocarriers with hydrophilic side chains, poly(ethylene oxide) (from YMER) and two amphoteric pairs having very specific acid-base properties: *N*-(3-dimethylaminopropyl)-*N,N*-diisopropanolamine (Jeffcat DPA) and L-lysine. In order to evaluate the pH-dependent amphoteric properties of the polymeric shell, we measured the Z-potential of the nanocapsules (P1-drug-loaded amphoteric NCs) at different pH values, ranging from 5.5 to 8. According to the graphic, the nanocapsules are

View Article Online
DOI: 10.1039/C6PY01275B



neutral at physiological conditions (pH= 7.4), since the carboxylate groups of L-lysine are neutralized with one of the tertiary amines of *N*-(3-dimethylaminopropyl)-*N,N*-diisopropanolamine. However, when the pH of the medium decreases to mimic the extracellular tumor microenvironment, the second tertiary amine becomes protonated and converts the nanocapsule into a cationic entity (Figure 3).

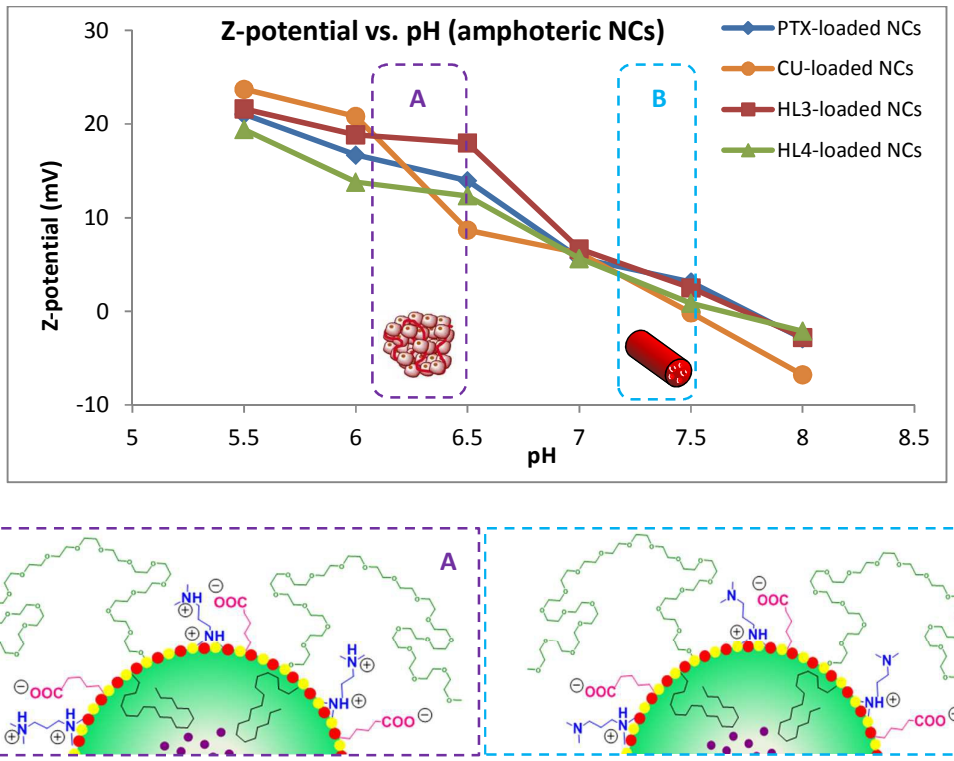


**Fig. 3**. Z-potential measurements at different pH conditions of paclitaxel-, curcumin-, HL3- and HL4-loaded nanocapsules (P1-drug-loaded amphoteric NCs). Surface charge at extracellular microenvironmental pH (a) and blood pH (b).

In order to further confirm the amphoteric behavior of the nanocapsules, we also prepared purely anionic and cationic versions of the nanocapsules, which only contained one of the amphoteric pairs: L-lysine for the anionic analogue and *N*-(3-dimethylaminopropyl)-*N,N*-diisopropanolamine for cationic analogue (P2-drug-loaded anionic NCs and P1-drug-loaded cationic NCs, respectively). In this case, regardless of the pH conditions, the nanocapsules lacking *N*-(3-dimethylaminopropyl)-*N,N*-diisopropanolamine presented an unchangeable anionic surface and those lacking L-lysine exhibited cationic characteristics. These results are shown in Figure S8 and Figure S9, respectively.

We have demonstrated that the specific design of the polymer is highly relevant, since it dictates the properties of the nanocarriers derived thereof. As mentioned above, the amphiphilic nature of the prepolymer shows the advantage that it can completely dissolve the

View Article Online
DOI: 10.1039/C6PY01275B



drug without external emulsifiers and consequently, the encapsulation efficiency (EE) and the drug loading (DL) content can be improved. These values were determined for the 4 nanoencapsulated drugs (Table 1), using the formulae shown in Figure S10.

| Encapsulated drug | EE (% wt.) | σ (% wt.) | DL (% wt.) | σ (% wt.) |
|---|---|---|---|---|
| Paclitaxel | 87.84 | 4.20 | 13.19 | 0.63 |
| Curcumin | 79.12 | 4.00 | 11.88 | 0.60 |
| HL3 | 96.97 | 0.83 | 9.71 | 0.08 |
| HL4 | 85.21 | 5.47 | 11.76 | 0.76 |

**Tab. 1**. Values for EE (%) and DL (%).

The table shows that the encapsulation efficiencies and drug loading contents for the nanoencapsulated drugs are high in all cases, being 79.12 ± 4.00 % and 9.71 ± 0.08 % the lowest values, respectively. These results are remarkable compared to other kinds of nanocarriers, such as liposomes and dendrimers, which generally exhibit lower entrapment efficiencies and limited encapsulation versatility.[40, 41] Moreover, some nanovehicles require the presence of external surfactants to guarantee the stability of the system, compromising the encapsulation efficiency and the drug loading content.[42] These external surfactants also lead to toxicological and allergic issues when administered intravenously. A well-known example is Cremophor® EL, which is a formulation vehicle used for various poorly-water soluble drugs, such as paclitaxel.[43-46]

Besides size, morphology and surface properties, shell biodegradability and specific cargo release are other essential properties of a delivery system. Thus, we also functionalized the polymeric wall with disulfide bonds that could be selectively cleaved by reductive enzymes and peptides overexpressed in the cytosolic environment of tumor cells. In our case, we chose reduced L-glutathione since it is an abundant reducing agent in living cells, with an intracellular concentration of 2-10 mM in certain organelles such as cytosol, and only 2-20 μM in blood and in extracellular matrix.[23, 24]

The *in-vitro* biodegradation of the nanocapsules was evaluated by TEM, DLS and Förster Resonance Energy Transfer (FRET). TEM and DLS experiments (Figure 4) were performed in a time course mode, taking samples before (control) and after 24, 48, 72 and 96 h the addition of 10 mM L-GSH.

View Article Online
DOI: 10.1039/C6PY01275B



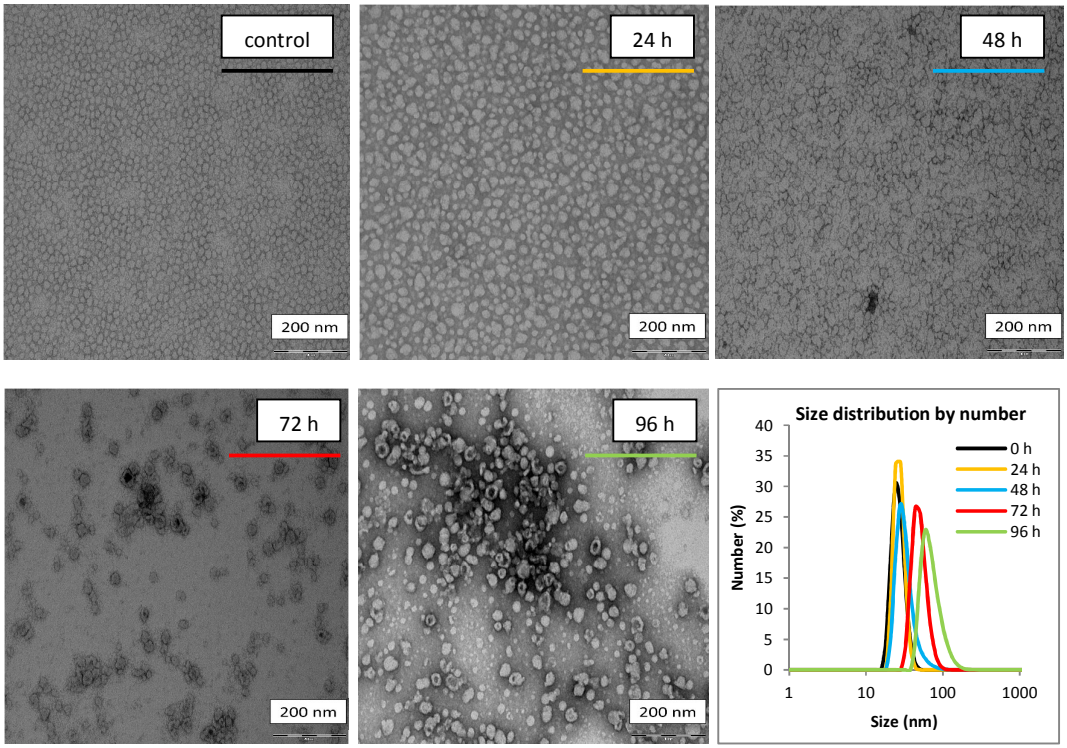


**Fig. 4**. TEM micrographs of control nanocapsules and nanocapsules treated with 10 mM L-GSH after 24 h, 48 h, 72 h and 96 h and DLS measurements of each sample.

TEM micrographs show that after 24 h the nanocapsules began to lose their homogeneity and started forming some larger entities. One day later, the sample became more heterogeneous and the nanocapsules lost their initial shape, leading to a non-structured polymeric material. After 3 days of incubation, the degraded polymers started organizing into aggregates and some of them presented holes in their structure, indicating extensive degradation. The last micrograph shows more accentuated physical transformations and aggregates growing to larger size. These results were confirmed by DLS measurements using the same conditions. In parallel, a sample of untreated nanocapsules was used to test their stability at 37 °C for 96 hours (Figure S11).

In order to confirm these observations, we performed FRET measurements to elucidate the release dynamics of two lipophilic tracers (DiO and DiI) from our nanocapsules under different conditions. FRET is a technique of particular interest due to its intrinsic sensitivity to small variations in molecular distance and orientation.[47, 48]

DiO- and DiI-loaded nanocapsules were mixed in the cuvette and the fluorescence was recorded at 37 °C and under constant stirring by exciting the sample at 484 nm and measuring the emission from 498 nm to 650 nm. FRET ratio was calculated as $I_a/(I_a+I_d)$, being $I_a$ the maximum intensity of the acceptor (DiI) and $I_d$ the maximum intensity of the donor (DiO). To

View Article Online
DOI: 10.1039/C6PY01275B



confirm that the increase of FRET was only caused by cargo release due to degradation of the polymeric wall, we recorded a few spectra before L-GSH addition.

Moreover, in order to confirm that our DDS would specifically release its content into the cytosol of cancer cells and avoid premature degradation and unspecific leakage of the drug, especially in the bloodstream, an experiment under similar conditions was performed using PBS and aqueous solutions of BSA and HSA (Figures S12 to Figure S15). These proteins were selected due to their relevant abundance in plasma and their exceptional binding capabilities as transporters. They can easily bind steroid hormones, thyroxine, tryptophan, several vitamins, metal ions and also drugs, facilitating their movement around the body or delivery to disposal sites. Thus, this protein can have a dramatic effect in the pharmacokinetics and pharmacodynamics of its transported agents. [49] The FRET ratios of the experiments are shown in Figure 5.

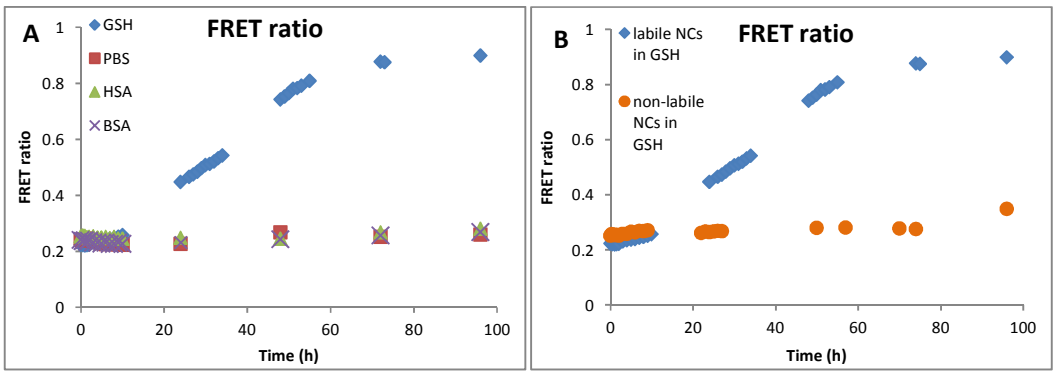


**Fig. 5**. A) Study of the FRET ratio of DiO- and DiI-loaded nanocapsules under different conditions (10 mM L-GSH, PBS, HSA, BSA) for 96 h. B) Study of the FRET ratio of labile and non-labile DiO- and DiI-loaded nanocapsules under reductive conditions (10 mM L-GSH) for 96 h.

In the case of the reductive medium, three different profiles could be identified and for each of them the slope was calculated (Figure S16). The release kinetics started with a slope of 0.0038 $h^{-1}$ and became more accentuated when the reductive tripeptide was added, reaching a slope of 0.0125 $h^{-1}$. Finally, the degradation profile became a plateau with a slope of 0.0010 $h^{-1}$, indicating that the whole content was virtually released.

Regarding PBS, we observed an invariably flat profile, indicating that there was no significant release of the nanoencapsulated molecules. The same behavior could be noticed when HSA and BSA were present in the solution medium (Figure S17 to Figure S19). Therefore, it can be confidently stated that the nanocapsules specifically release their content in a reductive medium containing L-GSH and that their crosslinked shell is robust enough to remain stable

View Article Online
DOI: 10.1039/C6PY01275B



and retain their cargo in aqueous or protein-rich solutions. In fact, polyurethane and polyurea bonds are known to be very stable against degradation,[50] especially if they are forming a crosslinked network. Thus, in order to prove that biodegradability was uniquely due to disulfide bonds present in the polymeric shell, we synthesized two versions of non-labile nanocapsules containing a drug and the same lipophilic tracers. Hence, we replaced DEDS by 1,6-hexanediol during the amphiphilic prepolymer preparation, since the latter is also a six membered monomer and could lead to comparable polymers. The degradation experiment was carried with non-labile DiO- and DiI-loaded nanocapsules under reductive conditions and measuring the FRET ratio over time. (Figure 5 and Figures S20 and Figure S21).

The FRET ratio observed is very low and only increases slightly after 4 days, with a slope of 0.0032 $h^{-1}$. Overall, this assay demonstrates the expected robustness of polyurethane/polyurea bonds along the polymeric shell that encloses the drug.

## 5. Conclusions

We have developed a versatile one-pot method to prepare specially designed prepolymers from industrial monomers, which have subsequently been used to nanoencapsulate different hydrophobic drugs in aqueous conditions. The potential of this system lies on the possibility of generating a wide range of prepolymers with very different physicochemical properties, by simply modifying the type and ratio of the starting monomers. In this line, the prepolymers can simultaneously be decorated with hydrophilic, hydrophobic, amphiphilic, cationic, anionic, amphoteric, labile and non-labile groups in one step, avoiding repeated purification cycles every time a functional group is introduced.

The specifically designed prepolymer is subsequently used to nanoencapsulate the desired hydrophobic drug in mild conditions and without surfactants, given its self-emulsifying nature. During this process, the components forming the prepolymer self-stratify according to the hydrophobic/hydrophilic gradient established from the inner core to the external surface. The composition of the synthesized prepolymer dictates the properties of the resulting nanocapsules. In this case, the nanocapsules loaded with different hydrophobic drugs show a controlled particle size distribution of approximately 20 nm, homogeneous and roughly round morphology, high encapsulation yield and good drug loading content. As a special feature, the shell exhibits a smart tunable surface responding to very small pH changes, being neutral to anionic at physiological pH and cationic at extracellular microenvironment pH. This response is

View Article Online
DOI: 10.1039/C6PY01275B



intended to favour its stealthiness in physiological conditions and to stimulate the nanocapsule penetration in tumor cells. Such dual behaviour is achieved with the coordinated effect of two specific ionomers present in the polymeric shell. Additionally, the nanocapsules show specific degradability through a redox-triggered process involving reduced L-GSH. The robustness of the system has been confirmed by DLS and FRET under different conditions and is due to the presence of polyurethane and polyurea bonds along the crosslinked polymeric network, which prevent premature leakage.

To our knowledge, this is the first time that multifunctionalized nanocapsules with high sensitivity to acidic tumor conditions and specific redox-triggered release are prepared through a one-pot process, by just combining the appropriate monomers that finally lead to self-organized nanocapsules.

*In vitro* and *in vivo* studies are underway.

## 6. Acknowledgements

This work was supported by Agència de Gestió d'Ajuts Univeristaris i de Recerca (2013 DI 028).

## 7. Notes and References

1 F. Bray, A. Jemal, N. Grey, J. Ferlay and D. Forman, *Lancet Oncol.*, 2012, **13**, 790-801.
2 R. L. Siegel, K. D. Miller and A. Jemal, *Ca-Cancer J. Clin.*, 2015, **65**, 5-29.
3 D. Farmakis, P. Stafylas, G. Giamouzis, N. Maniadakis and J. Parissis, *Int. J. Cardiol.*, 2016, **203**, 279-281.
4 F. Bray, *Cancer Epidemiol., Biomarkers Prev.*, 2016, **25**, 3-5.
5 J. Ferlay, I. Soerjomataram, R. Dikshit, S. Eser, C. Mathers, M. Rebelo, D. M. Parkin, D. Forman and F. Bray, *Int. J. Cancer*, 2015, **136**, E359-E386.
6 P. Workman and S. B. Kaye, *Trends Mol. Med.*, 2002, **8**, S1-S9.
7 C. G. Begley and L. M. Ellis, *Nature*, 2012, **483**, 531-533.
8 M. Ferrari, *Nat. Rev. Cancer*, 2005, **5**, 161-171.
9 W. Li, Y. Yang, C. Wang, Z. Liu, X. Zhang, F. An, X. Diao, X. Hao and X. Zhang, *Chem. Commun.*, 2012, **48**, 8120-8122.
10 S. Singh, A. Sharma and G. P. Robertson, *Cancer Res.*, 2012, **72**, 5663-5668.
11 I. Brigger, C. Dubernet and P. Couvreur, *Adv. Drug Delivery Rev.*, 2012, **64, Supplement**, 24-36.
12 L. Brannon-Peppas and J. O. Blanchette, *Adv. Drug Delivery Rev.*, 2004, **56**, 1649-1659.
13 J. Kost and R. Langer, *Adv. Drug Delivery Rev.*, 2012, **64, Supplement**, 327-341.
14 H. Wei, R.-X. Zhuo and X.-Z. Zhang, *Prog. Polym. Sci.*, 2013, **38**, 503-535.
15 A. De, R. Bose, A. Kumar and S. Mozumdar. *Targeted Delivery of Pesticides Using Biodegradable Polymeric Nanoparticles*, Springer India: New Delhi, 2014.
16 A. G. Cuenca, H. Jiang, S. N. Hochwald, M. Delano, W. G. Cance and S. R. Grobmyer, *Cancer*, 2006, **107**, 459-466.
17 P. Boisseau and B. Loubaton, *C. R. Phys.*, 2011, **12**, 620-636.

View Article Online
DOI: 10.1039/C6PY01275B



18 Z. Zuo, V. H. L. Lee and T. P. Begley. *Wiley Encyclopedia of Chemical Biology*, John Wiley & Sons, Inc.: 2007.
19 J. R. Sorolla and P. Rocas-Alonso. Method for the production of a microencapsulate, and corresponding reactive amphiphilic compound, microencapsulate and composition. 2014.
20 P. Rocas, M. Hoyos-Nogués, J. Rocas, J. M. Manero, J. Gil, F. Albericio and C. Mas-Moruno, *Adv. Healthcare Mater.*, 2015, **4**, 1956-1960.
21 P. Rocas, Y. Fernandez, S. Schwartz, I. Abasolo, J. Rocas and F. Albericio, *J. Mater. Chem. B*, 2015, **3**, 8421-8421.
22 C. Cuscó, J. Rocas, J. Garcia and E. Nicolás, *Rev. Soc. Cat. Quím.*, 2015, **15**, 25-36.
23 L. Zhu and V. P. Torchilin, *Integr. Biol.*, 2013, **5**, 96-107.
24 A. Latorre and A. Somoza, *Curr. Top. Med. Chem.*, 2014, **14**, 2662-2671.
25 R. F. Brissos, E. Torrents, F. Mariana dos Santos Mello, W. Carvalho Pires, E. de Paula Silveira-Lacerda, A. B. Caballero, A. Caubet, C. Massera, O. Roubeau, S. J. Teat and P. Gamez, *Metallomics*, 2014, **6**, 1853-1868.
26 L. V. Ratke, P.W., *Growth and Coarsening Ostwald Ripening in Material Processing*, 2002.
27 M. L. Immordino, F. Dosio and L. Cattel, *Int. J. Nanomed.*, 2006, **1**, 297-315.
28 R. Pignatello, A. Leonardi, R. Pellitteri, C. Carbone, S. Caggia, A. C. E. Graziano and V. Cardile, *Colloids Surf., A*, 2013, **434**, 136-144.
29 Y. Sheng, Y. Yuan, C. Liu, X. Tao, X. Shan and F. Xu, *J. Mater. Sci.: Mater. Med.*, 2009, **20**, 1881-1891.
30 V. C. F. Mosqueira, P. Legrand, J.-L. Morgat, M. Vert, E. Mysiakine, R. Gref, J.-P. Devissaguet and G. Barratt, *Pharm. Res.*, 2001, **18**, 1411-1419.
31 J. Fang, H. Nakamura and H. Maeda, *Adv. Drug Delivery Rev.*, 2011, **63**, 136-151.
32 V. Torchilin, *Adv. Drug Delivery Rev.*, 2011, **63**, 131-135.
33 H. Maeda, G. Y. Bharate and J. Daruwalla, *Eur. J. Pharm. Biopharm.*, 2009, **71**, 409-419.
34 U. Prabhakar, H. Maeda, R. K. Jain, E. M. Sevick-Muraca, W. Zamboni, O. C. Farokhzad, S. T. Barry, A. Gabizon, P. Grodzinski and D. C. Blakey, *Cancer Res.*, 2013, **73**, 2412-2417.
35 H. Maeda, H. Nakamura and J. Fang, *Adv. Drug Delivery Rev.*, 2013, **65**, 71-79.
36 V. Estrella, T. Chen, M. Lloyd, J. Wojtkowiak, H. H. Cornnell, A. Ibrahim-Hashim, K. Bailey, Y. Balagurunathan, J. M. Rothberg, B. F. Sloane, J. Johnson, R. A. Gatenby and R. J. Gillies, *Cancer Res.*, 2013, **73**, 1524-1535.
37 K. T. Oh, H. Yin, E. S. Lee and Y. H. Bae, *J. Mater. Chem.*, 2007, **17**, 3987-4001.
38 M. Wang, A. D. Miller and M. Thanou, *J. Drug Targeting*, 2013, **21**, 684-692.
39 A. Verma and F. Stellacci, *Small*, 2010, **6**, 12-21.
40 N. Mody, R. K. Tekade, N. K. Mehra, P. Chopdey and N. K. Jain, *AAPS PharmSciTech*, 2014, **15**, 388-399.
41 R. Gref, A. Domb, P. Quellec, T. Blunk, R. H. Müller, J. M. Verbavatz and R. Langer, *Adv. Drug Delivery Rev.*, 2012, **64, Supplement**, 316-326.
42 Y.-C. Kuo and H.-H. Chen, *Int. J. Pharm.*, 2009, **365**, 206-213.
43 K. Iwase, Y. Oyama, T. Tatsuishi, J.-y. Yamaguchi, Y. Nishimura, A. Kanada, M. Kobayashi, Y. Maemura, S. Ishida and Y. Okano, *Toxicol. Lett.*, 2004, **154**, 143-148.
44 J.-y. Yamaguchi, Y. Nishimura, A. Kanada, M. Kobayashi, K. Mishima, T. Tatsuishi, K. Iwase and Y. Oyama, *Toxicology*, 2005, **211**, 179-186.
45 D. Dye and J. Watkins, *Br. Med. J.*, 1980, **280**, 1353-1353.
46 J. Szebeni, C. R. Alving and F. M. Muggia, *J. Natl. Cancer Inst.*, 1998, **90**, 300-306.
47 R. M. Clegg, *Curr. Opin. Biotechnol.*, 1995, **6**, 103-110.
48 T. Ha, T. Enderle, D. F. Ogletree, D. S. Chemla, P. R. Selvin and S. Weiss, *Proc. Natl. Acad. Sci. USA*, 1996, **93**, 6264-6268.
49 S. Curry, *Vox Sang.*, 2002, **83**, 315-319.

View Article Online
DOI: 10.1039/C6PY01275B

50 E. Delebecq, J.-P. Pascault, B. Boutevin and F. Ganachaud, *Chem. Rev.*, 2013, **113**, 80-118.

View Article Online
DOI: 10.1039/C6PY01275B

## Table of Contents Entry

A one-pot versatile method for the preparation of sub-30 nm multisensitive polyurethane/polyurea nanocapsules with pH-synchronized shell cationization is presented. The nanocapsules have been loaded with different drugs which are released through a redox-triggered mechanism.